Book Chapter Template

Nematicity in electron-doped iron-pnictide superconductors

Hong-Yi Chen
hongyi@ntnu.edu.tw
Department of Physics, National Taiwan Normal University, Taipei, 116, Taiwan

Abstract

The nature of the nematicity in iron pnictides is studied with a proposed magnetic fluctuation. The spin-driven order in the iron-based superconductor has been realized in two categories – stripe SDW state and nematic state. The stripe SDW order opens a gap in the bans structure and causes a deformed Fermi surface. The nematic order does not make any gap in the band structure and still deforms the Fermi surface. The electronic mechanism of nematicity is discussed in an effective model by solving the self-consistent Bogoliubov-de Gennes equations. The nematic order can be visualized as a crisscross horizontal and vertical stripes. Both the stripes have the same period with different magnitude. The appearance of the orthorhombic magnetic fluctuations generates two uneven pairs of peaks at $(\pm\pi, 0)$ and $(0, \pm\pi)$ in its Fourier transformation. In addition, the nematic-order breaks the degeneracy of d_{xz} and d_{yz} orbitals and causes the elliptic Fermi surface near the Γ point. The spatial image of the local density of states reveals a $d_{x^2-y^2}$-symmetry form factor density wave.

Keywords: magnetic fluctuation, stripe SDW, nematic order, two-orbital, elliptic Fermi surface, LDOS maps

1. Introduction

The discovery of Fe-based superconductors with critical temperatures up to 55 K has begun a new era of investigations of the unconventional superconductivity. In common with copper-like superconductors (cuprate), the emergency of superconductivity in electron-doped Fe-pnictides such as $\mathrm{Ba\ Fe_{1-x}Co_xAs\ _2}$ is to suppress the magnetic order and fluctuations originated in the parent compound with $x = 0$ [1]. Of particular interests are the intertwined phases between the superconductivity and stripe spin density wave (SDW) order

(ferromagnetic stripes along one Fe-Fe bond direction that antiferromagnetically aligned along orthogonal Fe-Fe bond). In both pnictides and cuprates, the experimentally observed nematicity exists in an exotic phase between the superconductivity (SC) and the stripe SDW [2]. The nematicity, occurs in weakly doped iron-pnictides with tetragonal-to-orthorhombic structural transition [3-17], i.e., in a square unit cell, the point-group symmetry is reduced from C_4 (tetragonal) to C_2 (orthorhombic).

At present, there are two scenarios for the development of nematic order through the electronic configurations [18]. One scenario is the orbital fluctuations [19-23]. The structural order is driven by orbital ordering. The orbital ordering induces magnetic anisotropy and triggers the magnetic transition at a lower temperature. The other scenario is the spin fluctuations [24-27]. The magnetic mechanism for the structural order is associated with the onset of SDW.

Recently, Xingye Lu et. al. [28] reported that the low-energy spin excitations in underdoped sample $BaFe_{1.915}Ni_{0.085}As_2$change from C_4 symmetry to C_2 symmetry in the nematic state. Wenliang Zhang et. al. [29] exhibited that the reduction of the spin-spin correlation length at $(0,\pi)$ in $BaFe_{1.935}Ni_{0.065}As_2$ happens just below T_s, suggesting the strong effect of nematic order on low-energy spin fluctuations. Apparently, these experiments above have provided a spin driven nematicity-picture.

The partial melting of SDW has been proposed as the mechanism to explain the nematicity. The properties of the spin-driven nematic order have been studied in Landau-Ginzburg-Wilson's theory [18, 24-26]. Meanwhile, the lacks of the realistic microscopic model are responsible for the debates where the leading electronic instability, i.e., the onset of SDW causes the nematic order. Recently, an extended random phase approximation (RPA) approach in a five-orbital Hubbard model including Hund's rule interaction has shown that the leading instability is the SDW-driven nematic phase [30]. Although the establishment of the nematicity in the normal state has attracted a lot of attentions, the microscopic description of the nematic order and particularly, the relation between SC and the nematic order are still missing.

The magnetic mechanism for the structural order is usually referred to the Ising-nematic phase where stripe SDW order can be along the x–axis or the y–axis. The nematic phase is characterized by an underlying electronic order that the Z_2 symmetry between the x and y directions is broken above and the O(3) spin-rotational symmetry is preserved [25].

The magnetic configuration in FeSCs can be described in terms of two magnetic order parameters Δ_x and Δ_y. Both order parameters conventionally defined in momentum space are written as,

$$\Delta_\ell = \sum_k c^\dagger_{k+Q_\ell,\alpha}\sigma_{\alpha\beta}c_{k,\beta}\,, \qquad 1$$

where $\ell = x$ or y. Here the wave vectors $Q_x = \ \pi,0\ $ and $Q_y = \ 0,\pi\ $ correspond to the spins parallel along the y-axis and antiparallel along the x-axis, and the spins parallel along the x-axis and antiparallel along the y-axis, respectively.

In the stripe SDW state, the order parameters are set to $\langle\Delta_x\rangle \neq 0$ or $\langle\Delta_y\rangle \neq 0$, i.e., $\langle\Delta_\ell\rangle \neq 0$. This implies to choose a ordering vector either Q_x or Q_y. The Z_2 symmetry indicating to the degenerate of spin stripes along the y-axis

(corresponding to Q_x) or x-axis (corresponding to Q_y) is broken. In addition, the O(3) spin rotational symmetry is also broken. In the real space configuration, the magnetic ground state is an orthorhombic uniaxial stripe state. The stripe order reduces the point-group symmetry of a unit cell from C_4 (tetragonal) to C_2 (orthorhombic). In the nematic state, the order parameters are set to $\langle \Delta_x \rangle = \langle \Delta_y \rangle = 0$ and $\langle \Delta_x^2 \rangle \neq \langle \Delta_y^2 \rangle$. This implies that the magnetic fluctuations associated with one of the ordering vectors are stronger than the other $\langle \Delta_x^2 \rangle > \langle \Delta_y^2 \rangle$ or $\langle \Delta_y^2 \rangle > \langle \Delta_x^2 \rangle$. Therefore, the Z_2 symmetry is broken but the O(3) spin-rotational symmetry is not. In the real space configuration, the x and y directions of the magnetic fluctuations are inequivalent.

Recently, the reentrant C_4 symmetry magnetic orders have been reported in hole doped Fe-pnictide [27, 31, 32]. A double-Q order (choose both Q_x and Q_y) has been proposed to change the ground state from striped to tetragonal [33, 34]. Two stripe orders with the ordering vectors Q_x and Q_y are superposed to preserve the tetragonal symmetry. As a matter of fact, the nematic phase is characterized by an underlying electronic order that spontaneously breaks tetragonal symmetry. Since the double-Q order does not break the C_4 symmetry, it is not suitable to explain the nematicity.

The magnetic fluctuations trigger a transition from the tetragonal to orthorhombic phase. At very high temperature, $T > T_S$, $\langle \Delta_x \rangle = \langle \Delta_y \rangle = 0$ and the fluctuations of all order parameters have equal strength, i.e., $\langle \Delta_x^2 \rangle = \langle \Delta_y^2 \rangle$. As the temperature lowers, $T_N < T < T_S$, the thermodynamic average of order parameters still remain $\langle \Delta_x \rangle = \langle \Delta_y \rangle = 0$ but $\langle \Delta_x^2 \rangle \neq \langle \Delta_y^2 \rangle$. The fluctuations of one of the order Δ_x are on average different from the fluctuations of the other order Δ_y implying a broken Z_2 symmetry and a preserved O(3) symmetry. When the temperature is below T_N, the magnetic ground state is a stripe SDW state, i.e., $\langle \Delta_x \rangle = 0$ or $\langle \Delta_y \rangle = 0$.

In this chapter, we will exploit a two-orbital model to study the interplay between SC and nematicity in a two-dimensional lattice. The two-orbital model has been successfully used in many studies such as quasiparticle excitation, the density of states near an impurity [35, 36] and the magnetic structure of a vortex core [37].

2. Model

Superconductivity in the iron-pnictide superconductors originates from the FeAs layer. The Fe atoms form a square lattice and the As atoms are alternatively above and below the Fe-Fe plane. This leads to two sublattices of irons denoted by sublattices A and B. Many tight-binding Hamiltonians have been proposed to study the electronic band structure that include five Fe-3d orbitals [38], three Fe orbitals [39, 40], and simply two Fe bands [41-43]. Each of these models has its own advantages and range of convenience for calculations. For example, the five-orbital tight-binding model can capture all details of the DFT bands across the Fermi energy in the first Brillouin zone. However, in practice, it becomes a formidable task to solve the Hamiltonian with a large size of lattice in real space

even in the mean-field level. Several studies used five-orbital models in momentum space to investigate the single-impurity problem for different iron-based compounds such as $LaFeAsO_{1-x}F_x$, LiFeAs, and $K_xFe_{2-y}Se_2$. These studies confirmed that the detail of electronic bands strongly influences on the magnitude and location of the in-gap resonant states generated by the scattering of quasiparticles from single impurity [44-46].

On the other hand, the two-orbital models apparently have a numerical advantage dealing with a large size of lattice while retaining some of the orbital characters of the low-energy bands. Among the two-orbital (d_{xz} and d_{yz}) models, Zhang [47] proposed a phenomenological approach to takes into account the two Fe atoms per unit cell and the asymmetry of the As atoms below and above of the Fe plane. Later on, Tai and co-workers [48] improved Zhang's model by a phenomenological two-by-two-orbital model (two Fe sites with two orbitals each). The obtained low-energy electronic dispersion agrees qualitatively well with DFT in LDA calculations of the entire Brillouin zone of the 122 compounds.

The multi-orbital Hamiltonian of the iron-pnictide superconductors in a two-dimensional square lattice is described as,

$$H = \sum_{ijuv\alpha} t_{ijuv}\, c^{\dagger}_{iu\alpha} c_{jv\alpha} - \mu \sum_{iu\alpha} n_{iu\alpha} + U \sum_{iu} n_{iu\uparrow}\, n_{iu\downarrow} + \left(U' - \frac{J_H}{2}\right) \sum_{i,u<v,\alpha\beta} n_{iu\alpha}\, n_{iv\beta} - 2J_H \sum_{i,u<v} S_{iu} \cdot S_{iv} + J' \sum_{i,u\neq v} c^{\dagger}_{iu\uparrow} c^{\dagger}_{iu\downarrow} c_{iv\downarrow} c_{iv\uparrow}\,, \qquad 2$$

where

$$n_{iu\alpha} = c^{\dagger}_{iu\alpha} c_{iu\alpha}, \qquad 3$$

$$S_{iu} = \frac{1}{2} \sum_{\alpha\beta} c^{\dagger}_{iu\alpha} \sigma_{\alpha\beta} c_{iu\beta}\,, \qquad 4$$

with $\sigma_{\alpha\beta}$ the Pauli matrices. The operators $c^{\dagger}_{iu\alpha}$ ($c_{iu\alpha}$) create (annihilate) an ectron with spin $\alpha, \beta = \uparrow, \downarrow$ in the orbital $u, v = 1,2$ on the lattice site i; t_{ijuv} is the hopping matrix elements between the neighbor sites and μ is the chemical potential. U (U') is the intraorbital (interorbital) on-site interaction. The Hund's rule coupling is J_H and the pair hopping energy is J'. The spin-rotation invariance gives $U' = U - 2J_H$ and $J' = J_H$ [49]. Repulsion between electrons requires $J_H < U\,/\,3$.

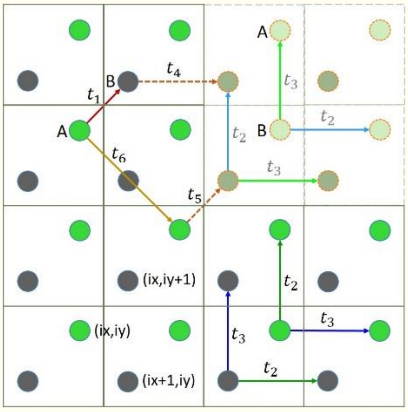

FIG. 1. (Color online) Two dimensional square lattice of the iron-based superconductors. There are two Fe atoms (green and grey color) in a unit cell and each atom have two orbitals. The bright color circle represents the first orbital and the faded color circle represents the second orbital. Solid lines indicate the hopping between the atoms in the same orbital and dashed lines indicate the hopping between the atoms in the different orbitals.

Here, we adopt Tai's phenomenological two-by-two-orbital model because it is able to deal with a large size of lattice in many aspects and the details of low-energy bands are similar to the results from DFT+LDA. In a two-orbital model, the hopping amplitudes are chosen as shown in Figure 1 [48] to fit the band structure from the first-principles calculations.

$$t_1 = t_{i,i\pm x\ y\ ,u,u} = -1, \qquad 5$$

$$\begin{cases} \dfrac{1+\ -1\ ^{x+y+u}}{2} t_2 + \dfrac{1-\ -1\ ^{x+y+u}}{2} t_3 = t_{i,i\pm\ x+y\ ,u,u} = 0.08 \\ \dfrac{1+\ -1\ ^{x-y+u}}{2} t_3 + \dfrac{1-\ -1\ ^{x-y+u}}{2} t_2 = t_{i,i\pm\ x-y\ ,u,u} = 1.35 \end{cases}, \qquad 6$$

$$t_4 = t_{i,i\pm\ x\pm y\ ,u,v\neq u} = -0.12, \qquad 7$$

$$t_5 = t_{i,i\pm x\ y\ ,u,v\neq u} = 0.09, \qquad 8$$

$$t_6 = t_{i,i\pm 2x\ 2y\ ,u,u} = 0.25, \qquad 9$$

where $u \neq v$ indicate two different ortibals.

Figure 1 shows the hopping parameters between unit cells and orbitals. For the same orbital, the hopping parameters t_2 and t_3 are chosen differently along the mutually perpendicular directions. The C_4 symmetry on the same orbital between different sublattices is broken. However, t_2 and t_3 are twisted for the different Fe atoms on the same sublattice which restore the C_4 symmetry of the lattice structure.

In the mean-field level,

$$\mathrm{H} = \mathrm{H}_0 + \mathrm{H}_\Delta + \mathrm{H}_{\mathrm{int}}, \qquad 10$$

the Hamiltonian is self-consistently solved accompanied with s^{+-}-wave superconducting order. The mean-field scheme is the same as Ref. [48].

$$\mathrm{H}_0 = \sum_{ijuv\alpha} t_{ijuv}\, c^{\dagger}_{iu\alpha} c_{jv\alpha} - \mu \sum_{iu\alpha} n_{iu\alpha}\,, \qquad 11$$

$$\mathrm{H}_{\Delta} = \sum_{iju\alpha\beta} \left(\Delta_{iju} c^{\dagger}_{iu\alpha} c^{\dagger}_{ju\beta} + \mathrm{h.c.} \right), \qquad 12$$

$$\mathrm{H}_{\mathrm{int}} = U \sum_{iu,\alpha\neq\beta} \langle n_{iu\beta} \rangle\, n_{iu\alpha} + U' \sum_{i,u<v,\alpha\neq\beta} \langle n_{iu\beta} \rangle\, n_{iv\alpha} + \; U' - J_H \sum_{i,u<v,\alpha} \langle n_{iu\alpha} \rangle\, n_{iv\alpha}. \qquad 13$$

The next nearest-neighbor intra-orbital attractive interaction V is responsible for the superconducting order parameter $\Delta_{iju} = V\langle c_{i\uparrow} c_{j\downarrow} \rangle$ [50-52]. According to the literatures where U is chosen to be 3.2 or less [48, 52], the magnetic configuration is a uniform SDW order. In order to make the stripe SDW order and the nematic order by changing electron doping, i.e., the chemical potential μ, we choose the parameters of interactions $U = 3.5$, $J_H = 0.4$, and $V = 1.3$ to induce a nematic order within a small doping range.

In momentum space, the spin configuration is determined by the order parameters Δ_x and Δ_y. The combination of these order parameters lack the visualization of the magnetic structure in real space. Therefore, we choose the staggered magnetization M_i in a lattice to study the states driven by the magnetic mechanism. The magnetic configuration is described as,

$$M_i = M_1 \cos(q_y \cdot r_i)\, e^{iQ_x \cdot r_i} + M_2 \sin\, q_x \cdot r_i \;\; e^{iQ_y \cdot r_i}, \qquad 14$$

where the wavevectors $q_x = \; 2\pi/\lambda\,, 0\;$ and $q_y = \; 0{,}2\pi/\lambda\;$ correspond to a modulation along the x-axis and the y-axis with wavelength λ. M_1 and M_2 are the amplitude of the modulation.

In the case of the absence of both q_x and q_y, M_i becomes

$$M_i = M_1 e^{iQ_x \cdot r_i} + M_2 e^{iQ_y \cdot r_i}, \qquad 15$$

As $M_1 = 0$ or $M_2 = 0$ are chosen, i.e., choosing the ordering vector either Q_x or Q_y, the state is a stripe SDW state. The existence of q_x and q_y does not affect the stripe SDW state. As two values of M_1 and M_2 are arbitrarily chosen, the spin configuration forms a stripe SDW along the $\;1{,}1\;$ direction. The existence of q_x and q_y has a lot of influences on the nematic state.

In the nematic state, the presences of both Q and q ordering vectors are necessary. Unlike the double-Q model, with the choice $M_1 \neq M_2$, the magnitudes of the modulated antiparallel spins along the x-axis and the y-axis are different due to the existence of q vectors. The magnetic configuration is attributed to two inequivalent stripes interpenetrating each other and formed a checked pattern. The checked pattern has the same period along the x- and y- direction. The period is determined by the value of q in the periodic boundary conditions. The value of q, therefore, cannot be arbitrary and must commensurate the lattice to stabilize the modulation and lower the energy of the system. As two modulated stripes have no phase difference, the checked patter shows a s-wave-like symmetry. In addition, as the modulations have a phase shift of $\pi/2$, the checked pattern shows a d-wave-like symmetry.

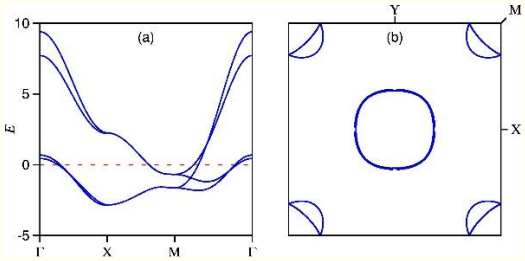

FIG. 2. (Color online) (a) and (b) are, respectively, the band structure and the Fermi surface without SDW. The Fermi energy (red dashed line) corresponds to the electron filling $n = 2.1$.

Figure 2 displays the Fermi surface and the band structure in the absence of SDW at the normal state, i.e., the superconductivity is set to zero. In the absence of SDW $U = 0$, the Hamiltonian in momentum space is,

$$\Psi^{\dagger} = \left(c^{\dagger}_{A1k\sigma} \quad c^{\dagger}_{A2k\sigma} \quad c^{\dagger}_{B1k\sigma} \quad c^{\dagger}_{B2k\sigma}\right), \qquad 16$$

$$\mathrm{H}_0 = \sum_{k\sigma} \Psi^{\dagger} \begin{pmatrix} \varepsilon_{A1} & \varepsilon_{12} & \varepsilon_{AB} & \varepsilon_c \\ \varepsilon_{12} & \varepsilon_{A2} & \varepsilon_c & \varepsilon_{AB} \\ \varepsilon_{AB} & \varepsilon_c & \varepsilon_{B1} & \varepsilon_{12} \\ \varepsilon_c & \varepsilon_{AB} & \varepsilon_{12} & \varepsilon_{B2} \end{pmatrix} \Psi\,, \qquad 17$$

where

$$\varepsilon_{A1} = -2t_3 \cos k_x - 2t_2 \cos k_y - 4t_6 \cos k_x \cos k_y\,, \qquad 18$$

$$\varepsilon_{A2} = -2t_2 \cos k_x - 2t_3 \cos k_y - 4t_6 \cos k_x \cos k_y\,, \qquad 19$$

$$\varepsilon_{B1} = -2t_2 \cos k_x - 2t_3 \cos k_y - 4t_6 \cos k_x \cos k_y\,, \qquad 20$$

$$\varepsilon_{B2} = -2t_3 \cos k_x - 2t_2 \cos k_y - 4t_6 \cos k_x \cos k_y\,, \qquad 21$$

$$\varepsilon_{12} = -2t_4 \cos k_x - 2t_4 \cos k_y\,, \qquad 22$$

$$\varepsilon_{AB} = -4t_1 \cos\frac{k_x}{2} \cos\frac{k_y}{2}, \qquad 23$$

$$\varepsilon_c = -4t_5 \cos\frac{k_x}{2} \cos\frac{k_y}{2}, \qquad 24$$

The eigenvalues are

$$E_{1,k} = \varepsilon_+ - \sqrt{\varepsilon_-^2 + \left(\varepsilon_{12} - \varepsilon_{AB}\right)^2} - \varepsilon_c - \mu, \qquad 25$$

$$E_{2,k} = \varepsilon_+ + \sqrt{\varepsilon_-^2 + \left(\varepsilon_{12} - \varepsilon_{AB}\right)^2} - \varepsilon_c - \mu, \qquad 26$$

$$E_{3,k} = \varepsilon_+ - \sqrt{\varepsilon_-^2 + \left(\varepsilon_{12} + \varepsilon_{AB}\right)^2} + \varepsilon_c - \mu, \qquad 27$$

$$E_{4,k} = \varepsilon_+ + \sqrt{\varepsilon_-^2 + \left(\varepsilon_{12} + \varepsilon_{AB}\right)^2} + \varepsilon_c - \mu, \qquad 28$$

where

$$\varepsilon_{\pm} = \frac{\varepsilon_{A1} \pm \varepsilon_{B1}}{2}. \quad 29$$

Figure 2(a) shows that two hole bands are around the Γ point and two electron bands are around the M point. There is no gap in the band structure where the superconductivity is able to open a gap. The nature of Fermi surface is revealed by the line at the Fermi energy crossing the band dispersion through $\Gamma - X - M - \Gamma$ points. Figure 2(b) displays that the Fermi surface contains two-hole pockets are centered at Γ point and two electron pockets are centered at M points. In addition, the Fermi surface also exhibits the C_4 symmetry of the lattice structure.

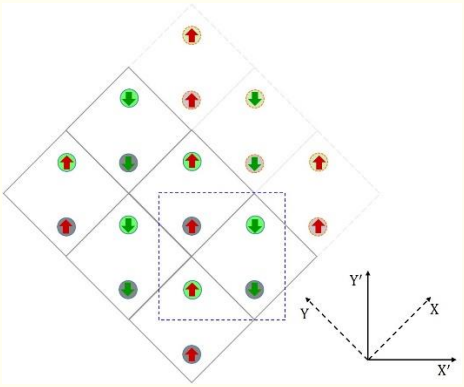

FIG. 3. (Color online) The schematic lattice structure of the Fe layer in the stripe SDW state. Blue dashed square denotes the four-Fe unit cell in the stripe SDW state.

In the stripe SDW state, the spin configuration is shown as Figure 3. The stripe SDW order enlarge the two-Fe unit cell to four-Fe unit cell as denoted by the blue dashed square in Figure 3. The antiferromagnetic order is along the X′ axis and the ferromagnetic order is along the Y′ axis. The magnetic unit cell (four-Fe unit cell) with lattice spacing $\sqrt{2}a$ and is oriented at a 45-degree angle with respect to the non-magnetic unit cell (two-Fe unit cell). The magnetic Brillouin zone is a square oriented at a 45-degree angle with respect to the crystal Brillouin zone. The size of the magnetic unit cell is twice of the nonmagnetic unit cell and the size of the magnetic Brillouin zone is half of the crystal Brillouin zone. The Hamiltonian in momentum space is

$$\widetilde{\Psi}_k^{\dagger} = \left(c^{\dagger}_{A_1^{\,1}\,k} \quad c^{\dagger}_{A_1^{\,2}\,k} \quad c^{\dagger}_{B_1^{\,1}\,k} \quad c^{\dagger}_{B_1^{\,2}\,k} \quad c^{\dagger}_{B_2^{\,1}\,k} \quad c^{\dagger}_{B_2^{\,2}\,k} \quad c^{\dagger}_{A_2^{\,1}\,k} \quad c^{\dagger}_{A_2^{\,2}\,k} \right), \quad 30$$

$$\mathrm{H} = \sum_k \widetilde{\Psi}_k^{\dagger} \cdot \mathbf{h} \cdot \widetilde{\Psi}_k, \quad 31$$

$$\mathbf{h}=\begin{pmatrix}
\varepsilon_{A_1^1} & 0 & \varepsilon_{t_1^x} & \varepsilon_{t_5^x} & \varepsilon_{t_1^y} & \varepsilon_{t_5^y} & \varepsilon_{t_{23}} & \varepsilon_{t_4} \\
0 & \varepsilon_{A_1^2} & \varepsilon_{t_5^x} & \varepsilon_{t_1^x} & \varepsilon_{t_5^y} & \varepsilon_{t_1^y} & \varepsilon_{t_4} & \varepsilon_{t_{32}} \\
\varepsilon_{t_1^x} & \varepsilon_{t_5^x} & \varepsilon_{B_1^1} & 0 & \varepsilon_{t_{32}} & \varepsilon_{t_4} & \varepsilon_{t_1^y} & \varepsilon_{t_5^y} \\
\varepsilon_{t_5^x} & \varepsilon_{t_1^x} & 0 & \varepsilon_{B_1^2} & \varepsilon_{t_4} & \varepsilon_{t_{23}} & \varepsilon_{t_5^y} & \varepsilon_{t_1^y} \\
\varepsilon_{t_1^y} & \varepsilon_{t_5^y} & \varepsilon_{t_{32}} & \varepsilon_{t_4} & \varepsilon_{B_2^1} & 0 & \varepsilon_{t_1^x} & \varepsilon_{t_5^x} \\
\varepsilon_{t_5^y} & \varepsilon_{t_1^y} & \varepsilon_{t_4} & \varepsilon_{t_{23}} & 0 & \varepsilon_{B_2^2} & \varepsilon_{t_5^x} & \varepsilon_{t_1^x} \\
\varepsilon_{t_{23}} & \varepsilon_{t_4} & \varepsilon_{t_1^y} & \varepsilon_{t_5^y} & \varepsilon_{t_1^x} & \varepsilon_{t_5^x} & \varepsilon_{A_2^1} & 0 \\
\varepsilon_{t_4} & \varepsilon_{t_{32}} & \varepsilon_{t_5^y} & \varepsilon_{t_1^y} & \varepsilon_{t_5^x} & \varepsilon_{t_1^x} & 0 & \varepsilon_{A_2^2}
\end{pmatrix}, \tag{32}$$

where

$$\varepsilon_{t_1^x}=-2t_1\cos k_x=-2t_1\cos\left(\frac{k_{x'}}{\sqrt{2}}\right), \tag{33}$$

$$\varepsilon_{t_1^y}=-2t_1\cos k_y=-2t_1\cos\left(\frac{k_{y'}}{\sqrt{2}}\right), \tag{34}$$

$$\varepsilon_{t_5^x}=-2t_5\cos k_x=-2t_5\cos\left(\frac{k_{x'}}{\sqrt{2}}\right), \tag{35}$$

$$\varepsilon_{t_5^y}=-2t_5\cos k_y=-2t_5\cos\left(\frac{k_{y'}}{\sqrt{2}}\right), \tag{36}$$

$$\begin{aligned}\varepsilon_{t_{23}}&=-2t_2\cos(k_x+k_y)-2t_3\cos(k_x-k_y)\\&=-2t_2\cos\left(\frac{k_{x'}}{\sqrt{2}}+\frac{k_{y'}}{\sqrt{2}}\right)-2t_3\cos\left(\frac{k_{x'}}{\sqrt{2}}-\frac{k_{y'}}{\sqrt{2}}\right),\end{aligned} \tag{37}$$

$$\begin{aligned}\varepsilon_{t_{32}}&=-2t_3\cos(k_x+k_y)-2t_2\cos(k_x-k_y)\\&=-2t_3\cos\left(\frac{k_{x'}+k_{y'}}{\sqrt{2}}\right)-2t_2\cos\left(\frac{k_{x'}-k_{y'}}{\sqrt{2}}\right),\end{aligned} \tag{38}$$

$$\varepsilon_{t_4}=-2t_4\cos(k_x+k_y)-2t_4\cos(k_x-k_y)=-4t_4\cos\frac{k_{x'}}{\sqrt{2}}\cos\frac{k_{y'}}{\sqrt{2}}, \tag{39}$$

$$\begin{aligned}\varepsilon_{t_6}&=-2t_6\cos 2k_x-2t_6\cos 2k_y\\&=-2t_6\cos\sqrt{2}k_{x'}-2t_6\cos\sqrt{2}k_{y'}\end{aligned} \tag{40}$$

$$\varepsilon_{A_1^1}=\varepsilon_{t_6}+U\langle n_{A_1^1k\downarrow}\rangle+U'\langle n_{A_1^2k\downarrow}\rangle+\ U'-J_H\ \langle n_{A_1^2k\uparrow}\rangle-\mu, \tag{41}$$

$$\varepsilon_{A_1^2}=\varepsilon_{t_6}+U\langle n_{A_1^2k\downarrow}\rangle+U'\langle n_{A_1^1k\downarrow}\rangle+\ U'-J_H\ \langle n_{A_1^1k\uparrow}\rangle-\mu, \tag{42}$$

$$\varepsilon_{B_1^1}=\varepsilon_{t_6}+U\langle n_{B_1^1k\downarrow}\rangle+U'\langle n_{B_1^2k\downarrow}\rangle+\ U'-J_H\ \langle n_{B_1^2k\uparrow}\rangle-\mu, \tag{43}$$

$$\varepsilon_{B_1^2}=\varepsilon_{t_6}+U\langle n_{B_1^2k\downarrow}\rangle+U'\langle n_{B_1^1k\downarrow}\rangle+\ U'-J_H\ \langle n_{B_1^1k\uparrow}\rangle-\mu. \tag{44}$$

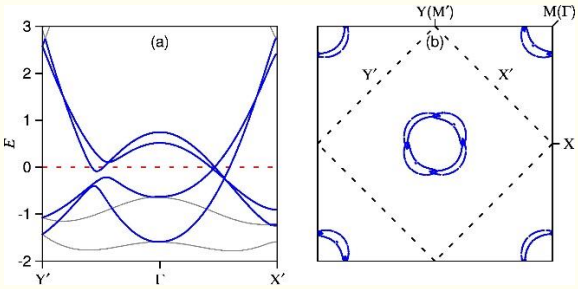

FIG. 4. (Color online) (a) and (b) are, respectively, the band structure and the Fermi surface in the stripe SDW state. The Fermi energy (red dashed line) corresponds to the electron filling $n = 2.04$. X′ and Y′indicate the magnetic Brillouin zone of the stripe SDW state.

According to the itinerant picture, the interactions between two sets of pockets give rise to a SDW order at the wave vector connecting them with $Q_x = \pi, 0$ or $Q_y = 0, \pi$. For example, as choosing the ordering vector Q_x, the spin configuration has antiparallel spins along the X′-direction and parallel spins along the Y′-direction [35]. The antiferromagnetism causes the gapless structure along the X′-direction and the ferromagnetism opens a gap along the Y′-direction, as shown in Figure 4(a). There are four pockets centered at the Γ point and two pockets long the $\Gamma - \mathrm{Y}'$ direction are inequivalent to the other two pockets along the $\Gamma - \mathrm{X}'$ direction. The C_2 symmetry of the Fermi surface resulting from the SDW gap is shown in Figure 4(b).

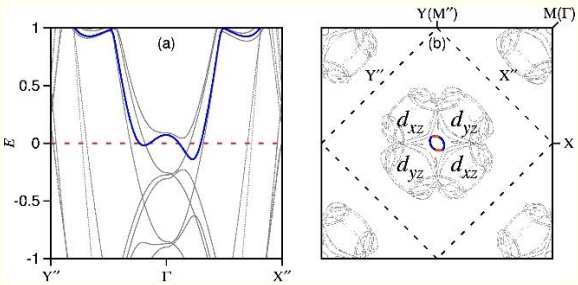

FIG. 5. (Color online) (a) and (b) are, respectively, the band structure and the Fermi surface in the nematic state. The asymmetric band (blue color) is responsible for the elliptic Fermi surface around the Γ point. The blue and red solid curves represent the major contributions from the orbitals d_{xz} and d_{yz}, respectively. The chemical potential is chosen as the electron filling $n = 2.1$. X′′ and Y′′indicate the magnetic Brillouin zone of the nematic state.

In the nematic state, the antiparallel spins along both the X′′ and Y′′ directions. The nematic unit cell is oriented at a 45 degree with respect to the nonmagnetic unit cell. The nematic Brillouin zone is also a square oriented at a 45 degree angle with respect to the crystal Brillouin zone. Since the antiferromagnetism are along both the X′′ and Y′′ directions, there is no gap in the band structure. In addition, as $M_1 < M_2$, the bands along the Y′′ direction are lifted higher and cause the bands asymmetric with respect to the Γ point. The

asymmetric bands result in deformed Fermi surfaces near the Γ point. As shown in Figure 5(a), the blue curve in the band structure forms an elliptic hole-pocket Fermi surface. Furthermore, the elliptic Fermi surface results from the unequal contribution of two orbitals d_{xz} and d_{yz}. The mechanism behind the fluctuations of d_{xz} and d_{yz} orbitals can be understood from an extended RPA approach where d_{xz}, d_{yz}, and d_{xy} orbitals equally contribute to the SDW instability, and in particular the d_{xy} orbital play a strong role in the nematic instability [30]. The nematic instability breaks the degeneracy of two orbitals d_{xz} and d_{yz} and causes the unequal charge distributions $n_{xz}(k)$ and $n_{yz}(k)$. The C_2-symmetry of the Fermi surface results from the degeneracy broken of two orbitals d_{xz} and d_{yz} (blue and red curves in Figure 5(b)).

Recently, N. Qureshi et. al. [53], Chong Wang et. al. [54], P. Steffens et. al. [55], and Huiqian Luo et. al. [56] pointed out that in-plane spin excitations exhibiting a large gap and indicating that the spin anisotropy is caused by the contribution of itinerant electrons and the topology of Fermi surface. These experiments indicate that the elliptic spin fluctuations at low energy in iron pnictides are mostly caused by the anisotropic damping of spin waves within FeAs-plane and the topology of Fermi surface. The degeneracy of orbitals will introduce the single ion anisotropy in spin fluctuations.

3. Visualize nematicity in a lattice

To visualize the nematicity in a lattice, we self-consistently solve the Bogoliubov-de Gennes (BdG) equations for the nematic state in a two-dimensional square lattice:

$$\sum_{jv}\begin{pmatrix} h_{ijuv\uparrow} & \Delta_{ijuv} \\ \Delta^*_{ijuv} & h^*_{iju\downarrow}\end{pmatrix}\begin{pmatrix} u^n_{ju\uparrow} \\ v^n_{juv\downarrow}\end{pmatrix} = E_{n\uparrow}\begin{pmatrix} u^n_{iu\uparrow} \\ v^n_{iu\downarrow}\end{pmatrix}, \qquad 45$$

where

$$h_{ijuv\alpha} = t_{ijuv\alpha} + \{-\mu + U\langle n_{iu\beta}\rangle + U'\langle n_{iv\beta}\rangle + \ U' - J_H\ \langle n_{iv\alpha}\rangle\}\delta_{ij}, \qquad 46$$

and $U' = U - 2J_H$. The self-consistency conditions are

$$\langle n_{iu\uparrow}\rangle = \sum_n {u^n_{iu\uparrow}}^2 f\ E_n\ , \qquad 47$$

$$\langle n_{iu\downarrow}\rangle = \sum_n {v^n_{iu\downarrow}}^2 [1 - f\ E_n\ ], \qquad 48$$

$$\Delta_{ijuv} = \frac{V}{2}\sum_n u^n_{iu\uparrow} v^{n*}_{iu\downarrow} \tanh\left(\frac{\beta E_n}{2}\right). \qquad 49$$

Here, $f(E_n)$ is the Fermi distribution function.

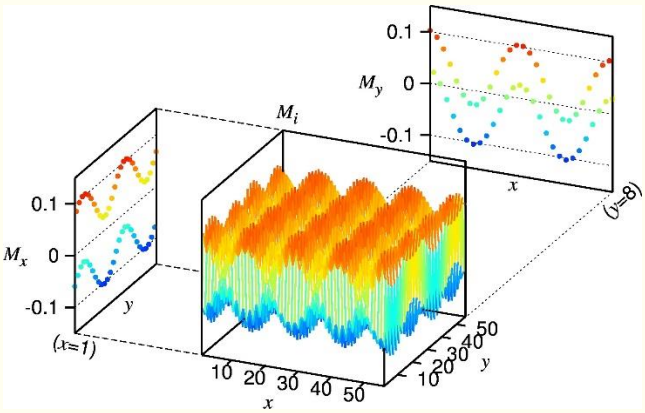

FIG. 6. (Color online) The real space configurations of the magnetization M_i are plotted on a 56×56 square lattice. The left and the right panels are the sliced profile along the peaks along the y- and x-directions, respectively. Two curves show in both panels. The upper and lower curves represent the spin-up and spin-down configurations, respectively.

In Figure 6, we show the magnetic configuration in the coexisting state of the nematic order and SC. To view the detail of the structure, the slided profile along the peaks along the x- or y-direction are made (as shown on the sides of M_i in Figure 6). There are two sinusoidally modulated magnetizations on each paenl. The warm color and cold color modulations represent the spin-up modulation and the spin-down modulation, respectively. The amplitude of each modulation on the left and right panel corresponds to the value of M_1 and M_2. On the left panel, we have $M_1 \cos(q_y \cdot r_i) = 0.04 \cos(\frac{2\pi r_i}{28a})$ and on the right panel, we have $M_2 \cos(q_x \cdot r_i) = 0.06 \sin(\frac{2\pi r_i}{28a})$. Both modulations have the same period $28a$. Since $M_1 < M_2$, the configuration is orthorhombic and breaks the $90°$ rotational symmetry.

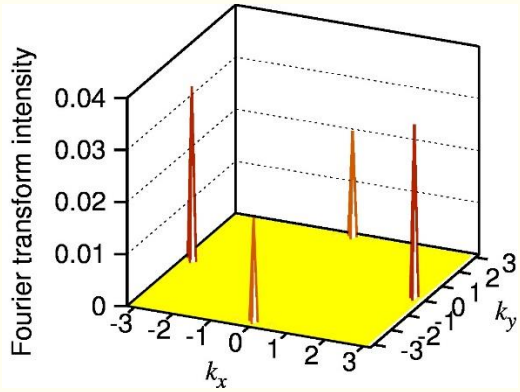

FIG. 7. (Color online) The Fourier transformation of the 56×56 spatial magnetic configuration.

Figure 7 shows the Fourier transformation of the spatial configuration of the nematic fluctuations. Two peaks appearing at $(\pm\pi, 0)$ corresponding to the ordering vector Q_x and two peaks exhibiting at $(0, \pm\pi)$ corresponding to the

ordering vector Q_y. We found that the intensities of peaks associated the ordering vector Q_x is greater than peaks associated the ordering vector Q_y, which is due to the unequal value of M_1 and M_2. The intensities of two peaks along the $k_x(k_y)$-direction have the same magnitude indicating $\langle\Delta_x\rangle = \langle\Delta_y\rangle = 0$. Moreover, the nonequivalence of the intensities between the k_x- and k_y-directions indicates $\langle\Delta_y^2\rangle > \langle\Delta_x^2\rangle$. Therefore, the modulated antiparallel spin configuration is the nematic state. These features are preserved even as the SC order is equal to zero. This result is in agreement with the neutron scattering experiments [3,10].

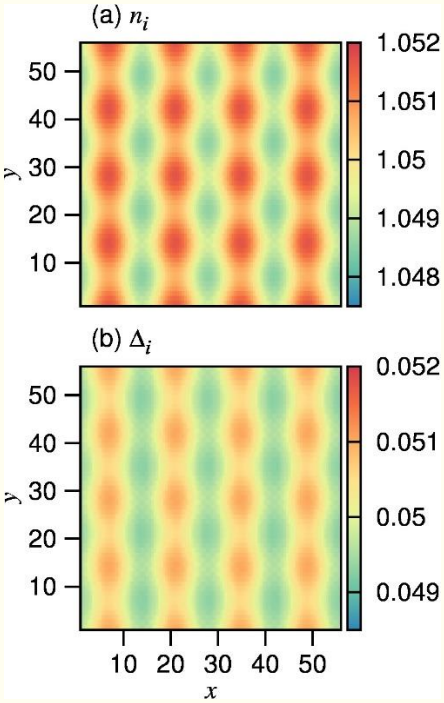

FIG. 8. (Color online) (a) The spatial configuration of the electronic charge density n_i. (b) The spatial configuration of the s^{+-}-wave superconducting order parameter Δ_i.

We further illustrate the electronic charge density $n_i = (n_{i\uparrow} + n_{i\downarrow})$ and the s^{+-}-wave SC order-parameter Δ_i as shown in Figure 8(a) and 8(b). Particularly, the nematicity of the spin order induces a modulated charge density wave (CDW) which does not occur in the stripe SDW state. The CDW consists of crisscrossed horizontal and vertical stripes. The amplitudes of the vertical stripes are larger than the horizontal stripes. Therefore, the CDW forms a checked pattern, instead of a checkerboard pattern. The stripes on both x- and y-directions have the same period 14*a* which is the half period of the magnetization.

Moreover, although the checked pattern of the CDW is two-fold symmetry, the CDW exhibits a $d_{x^2-y^2}$-symmetry, instead of a d_{xy}-symmetry (diagonal stripes crisscrossed pattern), form factor density wave. The space configuration

of the SC order parameter Δ_i shows the same features as the CDW order, as shown in Figure 8(b).

4. The local density of states

The local density of states (LDOS) proportional to the differential tunneling conductance as measured by STM is expressed as,

$$\rho_i\ E\ = -\frac{1}{N_x N_y}\sum_{nu}[\ u^n_{iu\uparrow}\ ^2 f'\ E_n - E\ +\ v^n_{iu\downarrow}\ ^2 f'\ E_n + E\ ]\,, \qquad 51$$

where $N_x \times N_y = 24 \times 24$ are the size of supercells.

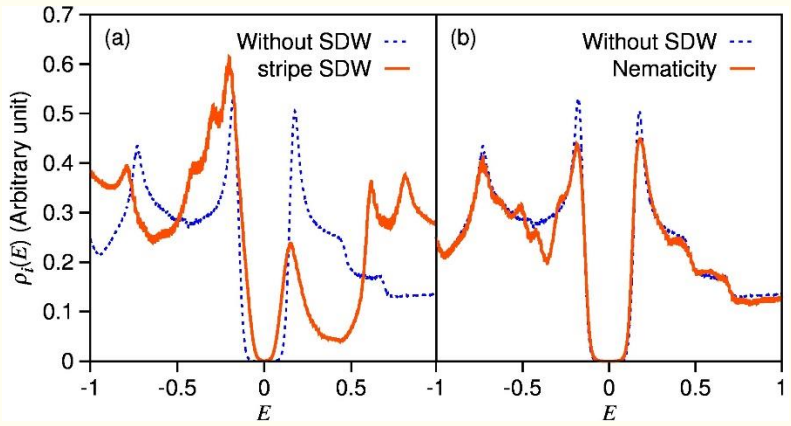

FIG. 9. (Color online) The LDOS in the (a) stripe SDW state and (b) nematic state. The dashed (blue) line represents the LDOS without magnetization ($M_i = 0$).

In the striped SDW state, spins are parallel in the y-direction and antiparallel in the x-direction and causes the gap and gapless features in the band structure, respectively. The SDW gap shifts toward negative energy and the coherence peak at the negative energy is pushed outside the SDW gap and enhanced. The coherence peak at the positive energy is moved inside the SDW gap and suppressed. This is a prominent feature caused by the magnetic SDW order that the intensities of superconducting coherence peaks are obvious asymmetry (as shown in Figure 9(a)) [57].

In the nematic state, spins are antiparallel in the x- and y- directions leading to a gapless feature in the band structure. The superconducting gap is the only gap appears in the LDOS. Moreover, comparing to the state without SDW, the competition between the nematic order and the superconducting order causes the slightly suppression of the coherence peaks. The feature of the suppression results in a dip at the negative energy outside the coherence peaks (as shown in Figure 9(b)).

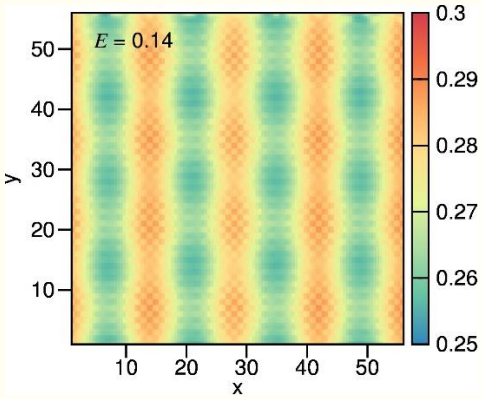

FIG. 10. (Color online) The LDOS map at $E = 0.14$ with $M_i \neq 0$.

Furthermore, Figure 10 displays a spatial distribution of LDOS, also known as LDOS map, at $E = 0.14$. The LDOS map shows the same features as the charge density distribution at the energy within the coherence peaks. The LDOS map exhibits a checked pattern, two-fold symmetric configuration, and $d_{x^2-y^2}$-symmetry form factor density wave. These features have not yet been reported by STM experiments.

It is worth to note that STM measurements by T.-M. Chuang et. al. [5] and M. P. Allan [58] reported that the dimension of the electronic nanostructure is around $8a$ and the nanostructure aligns in a unidirectional fashion. The highly two-fold symmetric structure of the QPI patterns is represented by using the Fourier transformation of the STS-imaging. Moreover, in cuprate, the more advanced measurement of the atomic-scale electronic structure has shown a d-wave like symmetry form factor density wave [59, 60]. There are four peaks appears around the center of the momentum space in the QPI patterns. Such an atomic-scale feature in cuprates has not yet been reported in iron-pnictides and in the nematic state.

5. Phase diagram

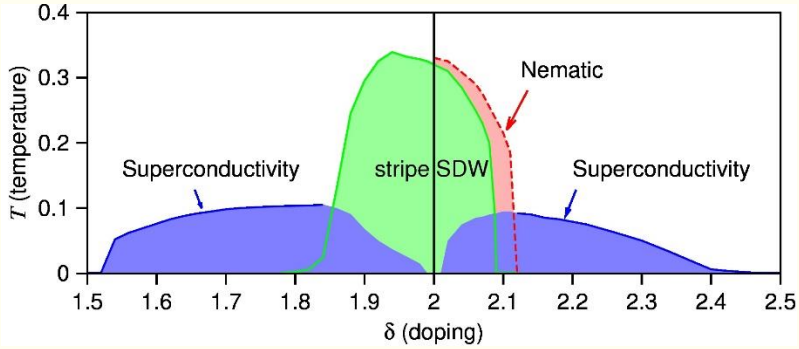

FIG. 11. (Color online) The phase diagram of the stripe SDW order (blue), nematic order (green) and superconducting order (red) as a function of doping.

To further verifying the spin configuration of the nematic order, a phase diagram is presented in Figure 11. In the phase diagram, the stripe SDW order, nematic order and s^{+-}-wave superconducting order as a function of doping are obtained from the self-consistent calculation to solve the BdG equations.

In the hole-doped region, the magnetization exhibits the stripe SDW order and drops dramatically around $n = 1.85$ and vanishes at $n = 1.80$. In the meantime, the s^{+-}-wave superconducting order reaches its maximal value at $n = 1.85$ and then gradually decreases.

In the electron-doped region, the stripe SDW order (green curve) has its maximal value at $n = 2.00$, then rapidly diminishes in a small region of doping, and finally reaches zero at $n = 2.09$. The superconductivity (blue curve) swiftly increases in a small region from $n = 2.02$ to $n = 2.04$, then reaches its maximal value at $n = 2.10$, and finally gradually decreases to almost zero around $n = 2.40$. The nematic state (red region) is in a small region next to the stripe SDW where the nematic trantition line (red dashed curve) tracks closely the stripe SDW transition line. The nematic order is favor to appear in the electron-doped regime, but not the hole-doped regime.

There are two regions where the stripe SDW coexist with the SC and the nematic order coexist with the SC. In the region where the stripe SDW coexist with the SC, the magnetic structure is an orthorhombic uniaxial stripe state. The ordering vector is either Q_x or Q_y implying $\langle \Delta_x \rangle = 0$ or $\langle \Delta_y \rangle = 0$. In the region where the nematic order coexist with the SC, the magnetic structure is a crisscrossed stripe state with two-fold symmetry. The ordering vectors are Q_x and Q_y associated with two modulating vectors q_x and q_y implying $\langle \Delta_x \rangle = \langle \Delta_y \rangle = 0$ and $\langle \Delta_x^2 - \Delta_y^2 \rangle \neq 0$ [62].

It is worth to note that the phase diagram of the electron-doped region is consistent with the Figure 1.3 of Kuo's thesis on $\mathrm{Ba\ Fe}_{1-x}\mathrm{Co}_x\mathrm{As}_{\ 2}$ [63]. Both figures show the same behavior of the nematic phase. Near optimally doped region under the superconducting dome, it is mentioned that the long range nematic order coexists with the superconductivity. However, such results still have not been reported from experiments. In addition, the magnetoresistivity of $\mathrm{Ba}_{0.5}\mathrm{K}_{0.5}\mathrm{Fe}_2\mathrm{As}_2$ reported a nematic superconducting state recently and suggested that the hole-doped superconductor is the mixture of s-wave and d-wave superconducting orders [64]. These results provide a different path to further researches to understand the mechanism of the nematic state in the superconductivity.

Conclusion(s)

The two-orbital Hamiltonian used in the iron-based superconductors has always been questioned its validity. Many studies have approved that a lot of the phenomena are attributed to d_{xz} and d_{yz} orbitals. In particular, d_{xz} and d_{yz} orbitals are responsible for the SDW instability.

The stripe SDW order opens a gap in the band structure and deforms the Fermi surface. However, the band structure of the nematic order is gapless and the Fermi surface is deformed to an ellipse. The mechanism can be understood

from the instability of SDW. The nematic order has visualized as a checked pattern formed by a crisscrossed modulated horizontal and vertical stripes. The inequivalent strengths of the horizontal and vertical stripe break the degeneracy of two orbitals d_{xz} and d_{yz} and cause an elliptic Fermi surface. The Fourier transformation of the orthorhombic structure of the magnetization shows two uneven pairs of peaks at $(\pm\pi,0)$ and $(0,\pm\pi)$. Moreover, the LDOS map shows a $d_{x^2-y^2}$-symmetry form factor density wave.

Finally, the nematic order is favor to exist in the electron-doped regime, but not the hole-doped regime.

Acknowledgments

H.Y.C. was supported by MoST of Taiwan under Grant MOST 107-2112-M-003-002 and National Center for Theoretical Science of Taiwan

References

[1] A. D. Christianson, E. A. Goremychkin, R. Osborn, S. Rosenkranz, M. D. Lumsden, C. D. Malliakas, I. S. Todorov, H. Claus, D. Y. Chung, M. G. Kanatzidis, R. I. Bewley, and T. Guidi, *Unconventional superconductivity in Ba0.6K0.4Fe2As2 from inelastic neutron scattering*, Nature 456, 930 (2008).

[2] J. C. Séamus Davis and Dung-Hai Lee, *Concepts relating magnetic interactions, intertwined electronic orders, and strongly correlated superconductivity*, PNAS 110, 17623 (2013).

[3] Jun Zhao, D. T. Adroja, Dao-Xin Yao, R. Bewley, Shiliang Li, X. F. Wang, G. Wu, X. H. Chen, Jiangping Hu, and Pengcheng Dai, *Spin waves and magnetic exchange interactions in CaFe2As2*, Nature Phys. 5, 555 (2009).

[4] Ming Yi, Donghui Lu, Jiun-Haw Chu, James G. Analytis, Adam P. Sorini, Alexander F. Kemper, Brian Moritz, Sung-Kwan Mo, Rob G. Moore, Makoto Hashimoto, Wei-Sheng Lee, Zahid Hussain, Thomas P. Devereaux, Ian R. Fisher, and Zhi-Xun Shen, *Symmetry-breaking orbital anisotropy observed for detwinned Ba(Fe1-xCox)2As2 above the spin density wave transition*, PNAS 108, 6878 (2011).

[5] T.-M. Chuang, M. P. Allan, Jinho Lee, Yang Xie, Ni Ni, S. L. Bud ' ko, G. S. Boebinger, P. C. Canfield, and J. C. Davis, *Nematic Electronic Structure in the "Parent" State of the Iron-Based Superconductor Ca(Fe1 –xCox)2As2*, Science 327, 181 (2010).

[6] Jiun-Haw Chu, James G. Analytis, Kristiaan De Greve, Peter L. McMahon, Zahirul Islam, Yoshihisa Yamamoto, and Ian R. Fisher, *In-Plane Resistivity Anisotropy in an UnderdopedIronArsenideSuperconductor*, Science 329, 824 (2010).

[7] Jiun-Haw Chu, James G. Analytis, David Press, Kristiaan De Greve, Thaddeus D. Ladd, Yoshihisa Yamamoto, and Ian R. Fisher, *In-plane electronic anisotropy in underdoped Ba(Fe1−xCox)2As2 revealed by partial detwinning in a magnetic field*, Phys. Rev. B 81, 214502 (2010).

[8] T. Shimojima, K. Ishizaka, Y. Ishida, N. Katayama, K. Ohgushi, T. Kiss, M. Okawa, T. Togashi, X.-Y. Wang, C.-T. Chen, S. Watanabe, R. Kadota, T. Oguchi, A. Chainani, and S. Shin, *Orbital-Dependent Modifications of Electronic Structure across the Magnetostructural Transition in BaFe2As2*, Phys. Rev. Lett. 104, 057002 (2010).

[9] M. A. Tanatar, E. C. Blomberg, A. Kreyssig, M. G. Kim, N. Ni, A. Thaler, S. L. Bud'ko, P. C. Canfield, A. I. Goldman, I. I. Mazin, and R. Prozorov, *Uniaxial-strain mechanical*

detwinning of CaFe2As2 and BaFe2As2 crystals: Optical and transport study, Phys. Rev. B 81, 184508 (2010).
[10] L. W. Harriger, H. Q. Luo, M. S. Liu, C. Frost, J. P. Hu, M. R. Norman, and Pengcheng Dai, *Nematic spin fluid in the tetragonal phase of BaFe2As2*, Phys. Rev. B 84, 054544 (2011).
[11] M. Nakajima, T. Liang, S. Ishida, Y. Tomioka, K. Kihou, C. H. Lee, A. Iyo, H. Eisaki, T. Kakeshita, T. Ito, and S. Uchida, *Unprecedented anisotropic metallic state in undoped iron arsenide BaFe2As2 revealed by optical spectroscopy*, PNAS 108, 12238 (2011).
[12] Hsueh-Hui Kuo, Jiun-Haw Chu, Scott C. Riggs, Leo Yu, Peter L. McMahon, Kristiaan De Greve, Yoshihisa Yamamoto, James G. Analytis, and Ian R. Fisher, *Possible origin of the nonmonotonic doping dependence of the in-plane resistivity anisotropy of Ba(Fe1−xTx)2As2(T=Co, Ni and Cu)*, Phys. Rev. B 84, 054540 (2011).
[13] S. Kasahara, H. J. Shi, K. Hashimoto, S. Tonegawa, Y. Mizukami, T. Shibauchi, K. Sugimoto, T. Fukuda, T. Terashima, Andriy H. Nevidomskyy, and Y. Matsuda, *Electronic nematicity above the structural and superconducting transition in BaFe2(As1−xPx)2*, Nature 486, 382 (2012).
[14] Jiun-Haw Chu, Hsueh-Hui Kuo, James G. Analytis, and Ian R. Fisher, *Divergent Nematic Susceptibility in an Iron Arsenide Superconductor*, Science 337, 710 (2012).
[15] Rafael M. Fernandes, Anna E. Böhmer, Christoph Meingast, and Jörg Schmalian, *Scaling between Magnetic and Lattice Fluctuations in Iron Pnictide Superconductors*, Phys. Rev. Lett. 111, 137001 (2013).
[16] E. C. Blomberg, M. A. Tanatar, R. F. Fernandes, I. I. Mazin, B. Shen, H.-H. Wen, M. D. Johannes, J. Schmalian, and R. Prozorov, *Sign-reversal of the in-plane resistivity anisotropy in hole-doped iron pnictides*, Nature Comm. 4, 1914 (2013).
[17] C. Mirri, A. Dusza, S. Bastelberger, J.-H. Chu, H.-H. Kuo, I. R. Fisher, and L. Degiorgi, *Nematic-driven anisotropic electronic properties of underdoped detwinned Ba(Fe1−xCox)2As2 revealed by optical spectroscopy*, Phys. Rev. B 90, 155125 (2014).
[18] R. M. Fernandes, A. V. Chubukov and J. Schmalian, *What drives nematic order in iron-based superconductors?*, Nature Phys. 10, 97 (2014).
[19] Weicheng Lv and Philip Phillips, *Orbitally and magnetically induced anisotropy in iron-based superconductors*, Phys. Rev. B 84, 174512 (2011).
[20] Wei-Cheng Lee and Philip. W. Phillips, *Non-Fermi liquid due to orbital fluctuations in iron pnictide superconductors*, Phys. Rev. B 86, 245113 (2012).
[21] H. Z. Arham, C. R. Hunt, W. K. Park, J. Gillett, S. D. Das, S. E. Sebastian, Z. J. Xu, J. S. Wen, Z. W. Lin, Q. Li, G. Gu, A. Thaler, S. Ran, S. L. Bud'ko, P. C. Canfield, D. Y. Chung, M. G. Kanatzidis, and L. H. Greene, *Detection of orbital fluctuations above the structural transition temperature in the iron pnictides and chalcogenides*, Phys. Rev. B 85, 214515 (2012).
[22] Valentin Stanev and Peter B. Littlewood, *Nematicity driven by hybridization in iron-based superconductors*, Phys. Rev. B 87, 161122(R) (2013).
[23] Hiroyuki Yamase and Roland Zeyher, *Superconductivity from orbital nematic fluctuations*, Phys. Rev. B 88, 180502(R) (2013).
[24] R. M. Fernandes, A. V. Chubukov, J. Knolle, I. Eremin, and J. Schmalian, *Preemptive nematic order, pseudogap, and orbital order in the iron pnictides*, Phys. Rev. B 85, 024534 (2012).
[25] J. P. Hu and C. Xu, *Nematic orders in Iron-based superconductors*, Physica C 481, 215 (2012).
[26] R. M. Fernandes and J. Schmalian, *Manifestations of nematic degrees of freedom in the magnetic, elastic, and superconducting properties of the iron pnictides*, Supercond. Sci. Technol. 25, 084005 (2012).
[27] S. Avci, O. Chmaissem, J. M. Allred, S. Rosenkranz, I. Eremin, A.V. Chubukov, D. E. Bugaris, D. Y. Chung, M. G. Kanatzidis, J.-P Castellan, J. A. Schlueter, H. Claus, D. D.

Khalyavin, P. Manuel, A. Daoud-Aladine, R. Osborn, *Magnetically driven suppression of nematic order in an iron-based superconductor*, Nature Comm. 5, 3845 (2014).
[28] Xingye Lu, J. T. Park, Rui Zhang, Huiqian Luo, Andriy H. Nevidomskyy, Qimiao Si, Pengcheng Dai, *Nematic spin correlations in the tetragonal state of uniaxial-strained BaFe2−xNixAs2*, Science 345, 657 (2014).
[29] Wenliang Zhang, J. T. Park, Xingye Lu, Yuan Wei, Xiaoyan Ma, Lijie Hao, Pengcheng Dai, Zi Yang Meng, Yi-feng Yang, Huiqian Luo, and Shiliang Li, *Effect of Nematic Order on the Low-Energy Spin Fluctuations in Detwinned BaFe1.935Ni0.065As2*, Phys. Rev. Lett. 117, 227003 (2016).
[30] Morten H. Christensen, Jian Kang, Brian M. Andersen, and Rafael M. Fernandes, *Spin-driven nematic instability of the multiorbital Hubbard model: Application to iron-based superconductors*, Phys. Rev. B 93, 085136 (2016).
[31] D. D. Khalyavin, S. W. Lovesey, P. Maneul, F. Kruger, S. Rosenkranz, J. M. Allred, O. Chmaissem, and R. Osborn, *Symmetry of reentrant tetragonal phase in Ba1−xNaxFe2As2: Magnetic versus orbital ordering mechanism*, Phys. Rev. B 90, 174511 (2014).
[32] A. E. Böhmer, F. Hardy, L. Wang, T. Wolf, P. Schweiss, C. Meingast, *Superconductivity-induced re-entrance of the orthorhombic distortion in Ba1−xKxFe2As2*, Nature Comm. 6, 7911 (2015).
[33] Xiaoyu Wang, Jian Kang, Rafael M. Fernandes, *Magnetic order without tetragonal-symmetry-breaking in iron arsenides: Microscopic mechanism and spin-wave spectrum*, Phys. Rev. B 91, 024401 (2015).
[34] Maria N. Gastiasoro and Brian M. Andersen, *Competing magnetic double-Q phases and superconductivity-induced reentrance of C2 magnetic stripe order in iron pnictides*, Phys. Rev. B 92, 140506(R) (2015).
[35] Lihua Pan, Jian Li, Yuan-Yen Tai, Matthias J. Graf, Jian-Xin Zhu, and C. S. Ting, *Evolution of the Fermi surface topology in doped 122 iron pnictides*, Phys. Rev. B 88, 214510 (2013).
[36] YuanYuan Zhao, Bo Li, Wei Li, Hong-Yi Chen, Kevin E. Bassler, and C. S. Ting, *Effects of single- and multi-substituted Zn ions in doped 122-type iron-based superconductors*, Phys. Rev. B 93, 144510 (2016).
[37] Yi Gao, Huai-Xiang Huang, Chun Chen, C. S. Ting, and Wu-Pei Su, *Model of Vortex States in Hole-Doped Iron-Pnictide Superconductors*, Phys. Rev. Lett. 106, 027004 (2011).
[38] Kazuhiko Kuroki, Seiichiro Onari, Ryotaro Arita, Hidetomo Usui, Yukio Tanaka, Hiroshi Kontani, and Hideo Aoki, *Unconventional Pairing Originating from the Disconnected Fermi Surfaces of Superconducting LaFeAsO1−xFx*, Phys. Rev. Lett. 101, 087004 (2008).
[39] Patrick A. Lee and Xiao-Gang Wen, *Spin-triplet p-wave pairing in a three-orbital model for iron pnictide superconductors*, Phys. Rev. B 78, 144517 (2008).
[40] Maria Daghofer, Andrew Nicholson, Adriana Moreo, and Elbio Dagotto, *Three orbital model for the iron-based superconductors*, Phys. Rev. B 81, 014511 (2010).
[41] A. B. Vorontsov, M. G. Vavilov, and A. V. Chubukov, *Interplay between magnetism and superconductivity in the iron pnictides*, Phys. Rev. B 79, 060508(R) (2009).
[42] S. Maiti, R. M. Fernandes, and A. V. Chubukov, *Gap nodes induced by coexistence with antiferromagnetism in iron-based superconductors*, Phys. Rev. B 85, 144527 (2012).
[43] D. Parker, M. G. Vavilov, A. V. Chubukov, and I. I. Mazin, *Coexistence of superconductivity and a spin-density wave in pnictide superconductors: Gap symmetry and nodal lines*, Phys. Rev. B 80, 100508 (2009).
[44] R. Beaird, I. Vekhter, and Jian-Xin Zhu, *Impurity states in multiband s-wave superconductors: Analysis of iron pnictides*, Phys. Rev. B 86, 140507(R) (2012).
[45] A. Maisuradze and A. Yaouanc, *Magnetic form factor, field map, and field distribution for a BCS type-II superconductor near its Bc2(T) phase boundary*, Phys. Rev. B 87, 134508 (2013).

[46] Maria N. Gastiasoro, P. J. Hirschfeld, and Brian M. Andersen, *Impurity states and cooperative magnetic order in Fe-based superconductors*, Phys. Rev. B 88, 220509(R) (2013).
[47] Degang Zhang, *Nonmagnetic Impurity Resonances as a Signature of Sign-Reversal Pairing in FeAs-Based Superconductors*, Phys. Rev. Lett. 103, 186402 (2009).
[48] Y. Y. Tai, J.-X. Zhu, J. G. Matthias, and C. S. Ting, *Calculated phase diagram of doped BaFe2As2superconductor in a C4-symmetry breaking model*, Europhys. Lett. 103, 67001 (2013).
[49] C. Castellani, C. R. Natoli, and J. Ranninger, *Magnetic structure of V2O3 in the insulating phase*, Phys. Rev. B 18, 4945 (1978).
[50] P. Ghaemi, F. Wang, and A. Vishwanath, *Andreev Bound States as a Phase-Sensitive Probe of the Pairing Symmetry of the Iron Pnictide Superconductors*, Phys. Rev. Lett. 102, 157002 (2009).
[51] Xiaohang Zhang, Y. S. Oh, Y. Liu, L. Yan, K. H. Kim, R. L. Greene, and I. Takeuchi, *Observation of the Josephson Effect in Pb/Ba1−xKxFe2As2 Single Crystal Junctions*, Phys. Rev. Lett. 102, 147002 (2009).
[52] K. Seo, B. A. Bernevig, and J. Hu, *Pairing Symmetry in a Two-Orbital Exchange Coupling Model of Oxypnictides*, Phys. Rev. Lett. 101, 206404 (2008).
[53] N. Qureshi, P. Steffens, S. Wurmehl, S. Aswartham, B. Büchner, and M. Braden, *Local magnetic anisotropy in BaFe2As2: A polarized inelastic neutron scattering study*, Phys. Rev. B 86, 060410(R) (2012).
[54] Chong Wang, Rui Zhang, Fa Wang, Huiqian Luo, L. P. Regnault, Pengcheng Dai, and Yuan Li, *Longitudinal Spin Excitations and Magnetic Anisotropy in Antiferromagnetically Ordered BaFe2As2*, Phys. Rev. X 3, 041036 (2013).
[55] P. Steffens, C. H. Lee, N. Qureshi, K. Kihou, A. Iyo, H. Eisaki, and M. Braden, *Splitting of Resonance Excitations in Nearly Optimally Doped Ba(Fe0.94Co0.06)2As2: An Inelastic Neutron Scattering Study with Polarization Analysis*, Phys. Rev. Lett. 110, 137001 (2013).
[56] Huiqian Luo, Meng Wang, Chenglin Zhang, Xingye Lu, Louis-Pierre Regnault, Rui Zhang, Shiliang Li, Jiangping Hu, and Pengcheng Dai, *Spin Excitation Anisotropy as a Probe of Orbital Ordering in the Paramagnetic Tetragonal Phase of Superconducting BaFe1.904Ni0.096As2*, Phys. Rev. Lett. 111, 107006 (2013).
[57] Lihua Pan, Jian Li, Yuan-Yen Tai, Matthias J. Graf, Jian-Xin Zhu, and C. S. Ting, *Evolution of quasiparticle states with and without a Zn impurity in doped 122 iron pnictides*, Phys. Rev. B 90, 134501 (2014).
[58] M. P. Allan, T-M. Chuang, F. Massee, Yang Xie, Ni Ni, S. L. Bud'ko, G. S. Boebinger, Q. Wang, D. S. Dessau, P. C. Canfield, M. S. Golden & J. C. Davis, *Anisotropic impurity states, quasiparticle scattering and nematic transport in underdoped Ca(Fe1−xCox)2As2*, Nature Phys. 9, 220 (2013).
[59] Kazuhiro Fujita, Mohammad H. Hamidian, Stephen D. Edkins, Chung Koo Kim, Yuhki Kohsaka, Masaki Azuma, Mikio Takano, Hidenori Takagi, Hiroshi Eisaki, Shin-ichi Uchida, Andrea Allais, Michael J. Lawler, Eun-Ah Kim, Subir Sachdev, and J. C. Séamus Davis, *Direct phase-sensitive identification of a d-form factor density wave in underdoped cuprates*, PNAS 111,E3026 (2014).
[60] M. H. Hamidian, S. D. Edkins, Chung Koo Kim, J. C. Davis, A. P. Mackenzie, H. Eisaki, S. Uchida, M. J. Lawler, E.-A. Kim, S. Sachdev & K. Fujita, *Atomic-scale electronic structure of the cuprate d-symmetry form factor density wave state*, Nature Phys. 12, 150 (2016).
[61] Jiun-Haw Chu, James G. Analytis, Chris Kucharczyk, and Ian R. Fisher, *Determination of the phase diagram of the electron-doped superconductor Ba(Fe1−xCox)2As2*, Phys. Rev. B 79, 014506 (2009).
[62] Chung-Pin Chou, Hong-Yi Chen, C.S. Ting, *The nematicity induced d -symmetry charge density wave in electron-doped iron-pnictide superconductors*, Physica C 546, 61 (2018).

[63] Hsueh-Hui Kuo, ELECTRONIC NEMATICITY IN IRON-BASED SUPERCONDUCTORS [thesis]. Stanford University; 2014.
[64] Jun Li, Paulo J. Pereira, Jie Yuan, Yang-Yang Lv, Mei-Ping Jiang, Dachuan Lu, Zi-Quan Lin, Yong-Jie Liu, Jun-Feng Wang, Liang Li, Xiaoxing Ke, Gustaaf Van Tendeloo, Meng-Yue Li, Hai-Luke Feng, Takeshi Hatano, Hua-Bing Wang, Pei-Heng Wu, Kazunari Yamaura, Eiji Takayama-Muromachi, Johan Vanacken, Liviu F. Chibotaru, & Victor V. Moshchalkov, *Nematic superconducting state in iron pnictide superconductors*, Nature Comm. 8, 1880 (2017).